MINISTRY OF INDUSTRY AND TRADE
INDUSTRIAL UNIVERSITY OF HO CHI MINH CITY



NGUYEN VAN THOI

STUDY ON THE COMPLEXATION OF PLUMBAGIN WITH CR(III), TI(IV), HG(II) AND APPLICATIONS

Major: Chemical Engineering
Major code: 62520301

SUMMARY OF DOCTORATE THESIS

HO CHI MINH CITY, 2025

DRAFT

LIST OF PUBLISHED WORKS

I. International Journals (WoS/Scopus)

01.**Nguyen Van Thoi** , Tran Nguyen Minh An* , Nguyen Quoc Hung, Pham Van Tat , Le Van Tan* (2023), *"*The spectroscopic properties and capability of a new and selective complex of Ti-PLB for analyzing titanium in sand samples," *Microchemical Journal*, Vol. 194, pp. 109221. https://doi.org/10.1016/j.microc.2023.109221 (**Q1, IF=4.9**).

02.**Nguyen Van Thoi**, Do Thi Thao, Tran Nguyen Minh An*, Le Van Tan* (2025), *"*Synthesis, characterization and preliminary biological evaluation of novel Hg(PLB)2 and Cr(PLB)3 complexes," *Inorganic Chemistry Communications*, Vol. 177, pp. 114333, 2025. https://doi.org/10.1016/j.inoche.2025.114333 **(Q1, IF=4.4**).

03. **Nguyen Van Thoi**, Tran Khanh Luan, Tran Phuoc Vy, Tran Nguyen Minh An*, Le Van Tan* (2025), "Binding mechanism of $Cr(PLB)_3$ and $Hg(PLB)_2$ complexes with human serum albumin: spectroscopic, thermodynamic, and molecular docking investigations," *Results in Chemistry*, Vol. 16, pp. 102429. (**Q2**) https://doi.org/10.1016/j.rechem.2025.102429.

II. National Journals

01. Tran Nguyen Minh An, **Nguyen Van Thoi**[*], Nguyen Thi Kim Anh, Le Van Tan (2024), "Applicability of analysis, prediction of antidiabetic activity in silico docking-admet model and bioactivity based on $Ti(PLB)_2$ complex," *Tạp chí phân tích Hóa, Lý và Sinh học.* Tập 30, Số 01.

III. International Conferences

Le Van Tan, **Nguyen Van Thoi**, Tran Nguyen Minh An, "Inhibition of antidiabetic properties, biological activity and combination with prediction in silico Docking-Admet model base on $Ti(PLB)_2$ complex," *International*

Conference on Biomedical Chemistry and Applications - (ICBCA-24), Incheon, Sounth Korea, 2024.

IV. National Conferences

Nguyen Van Thoi, Tran Nguyen Minh An, Le Van Tan, "Novel Hg(II) - Plumbagin complexes: synthesis, properties, *in vitro* anti-cancer, anti-inflammatory, and alphaglucosidase inhibition activities and in silico study," *Hoá học xanh miền trung Tây nguyên lần thứ 2*, 2024.

Nguyen Van Thoi, Tran Nguyen Minh An, Le Van Tan, "Khả năng ứng dụng phân tích, dự báo hoạt tính kháng tiểu đường trong silico docking- Mô hình ADMET và hoạt tính sinh học dựa trên phức $Ti(PLB)_2$, *Hội thảo khoa học khao công nghệ Hoá học và Đại học Khoa học Huế,* 2024.

IV. Scientific Research Projects

STT	Project Title	Code	Level	Role	Implementation Time
1	Study on the complex of Plumbagin with Ti(IV) in solution and its applications	22/2H HSV01	University	Principal Investigator	2023
2	Complexes of Plumbagin with Hg(II), Cr(III): synthesis, complex properties, biological activities, and in silico molecular docking and simulation studies	24.1/H HSV05	University	Principal Investigator	2024

DRAFT

INTRODUCTION

Natural compounds, with their structural diversity and biological activities, have become the focus of research in medicinal chemistry, molecular biology, materials science, and analytical chemistry. Plumbagin (PLB, 5-hydroxy-2-methyl-1,4-naphthoquinone) has attracted attention due to its anticancer, anti-inflammatory, antibacterial, and antidiabetic activities; however, the metal complexes of PLB have been little studied [1][2]. Coordination with metal ions can alter the physicochemical and optical properties, solubility, stability, and even enhance the biological activity of PLB, opening up potential applications in sensing, analysis, and pharmacology.

Cr(III), Hg(II), and Ti(IV) are important transition metals: Cr(III) is related to the glucose tolerance factor (GTF), which helps regulate blood sugar; certain organic compounds of Hg(II) were once used in medicine; Ti(IV), with its derivative titanocene dichloride, has been investigated as a potential anticancer agent [3] [4]. Complexes of these three ions have been applied in analysis as reagents, indicators, or spectroscopic probes.

Currently, computational tools such as density functional theory (DFT), molecular docking, and molecular dynamics (MD) simulations are of great interest due to their ability to predict structures, binding energies, and ligand–protein interaction mechanisms, supporting the interpretation of experimental results.

On this basis, the dissertation entitled *"Study on the Complexation of PLB with Cr(III), Ti(IV), Hg(II) and Applications"* was conducted with the aims of investigating the formation of PLB complexes with these three ions in both solution and solid state; determining coordination ratios, optimal conditions, fluorescence emission/quenching mechanisms, and the relationship between structure and properties; as well as evaluating their biological interactions with human serum albumin (HSA) and enzymes by spectroscopic methods combined

DRAFT

with molecular docking, together with the anti-inflammatory, anticancer, and antidiabetic activities of the complexes.

The results were applied to the fluorescence determination of Ti(IV) and the quantification of Hg(II) by HPLC-DAD based on the $Hg(PLB)_2$ complex. The dissertation provides scientific data on the interactions of PLB with Cr(III), Ti(IV), and Hg(II), contributing to the development of optical reagents, analytical tools for heavy metals, and the orientation for research into biologically active drug candidates.

DRAFT

CHAPTER 1. LITERATURE REVIEW

Plumbagin (PLB, 5-hydroxy-2-methyl-1,4-naphthoquinone) is a natural naphthoquinone compound with an extended conjugated π-system, bearing a phenolic –OH group and two C=O groups at positions 1 and 4, which are favorable for coordinating metal ions to form stable six-membered chelate rings. PLB is an orange-yellow crystalline solid, soluble in polar organic solvents, and sensitive to light and pH [5],[6]. Metal coordination alters the electron distribution and $\pi \rightarrow \pi^*$, $n \rightarrow \pi^*$ transitions, leading to changes in optical absorption and emission, which form the basis for sensing applications. PLB exhibits anticancer, anti-inflammatory, antibacterial, and antidiabetic activities [7]; upon complexation, many studies have reported enhanced activity compared to free PLB [8].

Chapter 1 reviews the UV–Vis and fluorescence spectral characteristics of PLB, the effects of pH and solvents on λmax and emission intensity, and the mechanisms of fluorescence emission/quenching (PET, LMCT, ISC). The roles of –OH and C=O groups in coordination were analyzed, demonstrating the ability to form stable bidentate complexes, clearly evidenced by IR spectral shifts and fluorescence variations. Metal–PLB complexes of transition metals and rare earths have been reported, with some systems (e.g., $Cu(PLB)_2$, $Ln(PLB)_3$) exhibiting stronger anticancer and antioxidant activities than PLB, while certain nanostructured systems improved solubility and cellular selectivity. The synthesis of PLB complexes has been generally described in steps including dissolution, mixing, stirring/heating, precipitation, washing–drying, and characterization by UV–Vis, FT-IR, NMR, HR-MS, XRD, and XPS.

The dissertation also reviews the electronic properties, ionic radii, and coordination behavior of Ti(IV), Cr(III), and Hg(II). Ti(IV) is a hard acid with a d^0 configuration, favoring O-donor ligands and typically forming octahedral complexes. Cr(III) is a kinetically stable cation, usually forming octahedral complexes, absorbing in the visible region, and capable of quenching

DRAFT

fluorescence through LMCT/ISC processes. Hg(II) is a soft, highly polarizable acid with a heavy atom effect that enhances ISC and causes fluorescence quenching. In pharmacology, Ti(IV) has been investigated as a potential anticancer agent, Cr(III) is linked to blood glucose regulation and antidiabetic effects, and Hg(II), upon coordination, may inhibit enzymes or interact specifically with DNA.

In addition, Chapter 1 reviews the techniques employed in complex studies, such as UV–Vis, fluorescence, FT-IR, NMR, XPS, HR-MS, XRD, and TGA, which are used to determine structures, oxidation states, and electronic features. In silico methods including molecular docking, molecular dynamics (MD) simulations, and ADMET prediction were also introduced, playing important roles in predicting structures, binding energies, and elucidating interaction mechanisms with enzymes or target proteins.

Based on this review, the dissertation identifies the research gap concerning PLB complexes with Ti(IV), Cr(III), and Hg(II), focusing on their formation in solution and solid state, fluorescence emission/quenching mechanisms, structure–property relationships, and their potential applications in quantitative analysis as well as biological activity evaluation

DRAFT

CHAPTER 2. RESEARCH METHODS

2.1 Chemicals, instruments, and computational software

PLB (Sigma-Aldrich); solvents/reagents from Merck: ethanol, $Ti(NH_4)_2F_6$, HNO_3, HCl, NaOH, $CrCl_3$, $Hg(NO_3)_2$…; HSA (fatty acid–free), warfarin, ibuprofen (Sigma). All were of analytical grade and checked for purity.

Instruments: UV–Vis spectrophotometer HITACHI UH5300; fluorescence spectrometer HITACHI F-2700; FT-IR spectrometer Bruker Tensor 27; CD spectrometer Chirascan; HR-MS Agilent 6500 Q-TOF; pH meter Hanna HI 2210; HPLC–DAD Agilent 1260 (ZORBAX Eclipse Plus C18 column, 150 × 4.6 mm, 5 µm); filtration system, centrifuge, syringes.

Software: Gaussian 09/GaussView 6.0 (DFT, HOMO–LUMO, Mulliken/NBO); Discovery Studio 2020 (ligand/protein preparation, visualization); AutoDockTools 1.5.7 & AutoDock Vina (docking; AD4* parameter set); Schrödinger–Desmond v2022-4 (MD simulations).

2.2 Experimental methods

2.2.1 Preparation of solutions

Stock solution of PLB 1.0×10^{-3} M in ethanol (stored at 0–4 °C, protected from light); stock solutions of Cr(III), Ti(IV), Hg(II) 1.0×10^{-2} M (double-distilled water). Tris–HCl buffer 0.01 M (pH 6–9) for UV–Vis, fluorescence, and HSA interaction studies; pH adjusted with dilute HCl/NaOH. HSA solution 300 µM (phosphate buffer 10 mM, pH 7.4); warfarin/ibuprofen 6 mM (HPLC ethanol). Stock solutions of $Cr(PLB)_3$ and $Hg(PLB)_2$ complexes 1.0×10^{-3} M (DMSO, stored cold, protected from light).

2.2.2 UV–Vis and fluorescence studies

PLB (16–30 µM) in EtOH:H_2O (7:3, v/v), adjusted pH (5 or 9), measured UV–Vis absorption (200–800 nm). Fluorescence: PLB 30 µM in EtOH:H_2O (7:3), pH varied as studied.

$Ti(PLB)_2$: mix 2.0 mL PLB 100 µM + 0.1 mL Ti(IV) 1000 µM, make up to 10 mL (EtOH:H_2O 7:3, pH 5), equilibrate 5 min; measure at λex = 500 nm, λem = 605 nm.

$Cr(PLB)_3$, $Hg(PLB)_2$: 2.0–3.0 mL PLB 100 µM + 0.1 mL Cr(III)/Hg(II), make up to 10 mL (EtOH:H_2O 7:3, Tris pH 6.5), equilibrate 3 min; measure at λex = 310

nm, λem = 436 nm. Conditions: Hitachi F-2700, 1 cm quartz cuvette, scanning speed 1200 nm/min, PMT voltage 700 V, slit width 5 nm.

2.2.3 Fluorescence determination of Ti(IV) (Binh Thuan sand samples)

Sample digestion: HF/$HClO_4$ (sand bath) → HCl → adjust pH 5 (NH_3) → make up to 50 mL.Reagents: PLB 1.0×10^{-4} M (ethanol), Ti(IV) standard 1.0×10^{-3} M. Calibration curve: $0.1–0.8 \times 10^{-5}$ M Ti(IV) with PLB (pH 5), wait 5 min; measure at λex/λem 500/605 nm; calculate LOD/LOQ, R^2; check with standard addition, RSD%, and validate against ICP-OES.

2.2.4 Quantification of Hg(II) by HPLC–DAD

Principle: $Hg(PLB)_2$ complex absorbs in UV region, quantified by HPLC–DAD. Preparation: PLB 1.0×10^{-3} M (ethanol); Hg(II) standard 1000 mg/L; reaction: PLB 50 µM + Hg(II) 5–50 µM (Tris–HCl, EtOH:H_2O 7:3), incubated 5 min, filtered (0.22 µm). HPLC–DAD conditions: mobile phase EtOH:H_2O 5:5; flow rate 0.8 mL/min; 40 °C; detection λ = 224 nm; runtime 2–10 min. Calibration curve: peak area vs concentration; calculate LOD/LOQ, R^2, RSD%; compare with ICP-MS.

2.2.5 Evaluation of biological activities

Anticancer activity (MTT assay): HepG2, MCF-7, A549 cells (2.5–100 µM; 48 h); OD measured at 540 nm; calculate % viability and IC_{50} (TableCurve 2D).

α-Glucosidase inhibition: 96-well microplate with pNPG substrate; concentration range 4–500 µg/mL; OD measured at 405 nm; calculate % inhibition and IC_{50}.

Anti-inflammatory activity (NO inhibition): RAW 264.7 macrophages stimulated with LPS; nitrite (NO_2^-) quantified using Griess reaction (OD 540 nm); calculate % inhibition and IC_{50}.

Cytotoxicity on normal cells (HEK-293A, SRB assay): concentration range 0.032–20 µg/mL; OD 540 nm; IC_{50} determined, with ellipticine as positive control (+) and 1% DMSO as negative control (–); reference criterion $IC_{50} \leq 5$ µM.

All experiments were performed in accredited laboratories, following internationally published protocols.

DRAFT

CHAPTER 3 RESULTS AND DISCUSSION

3.1 Characteristics of PLB complexes with Cr(III), Hg(II), and Ti(IV) in solution

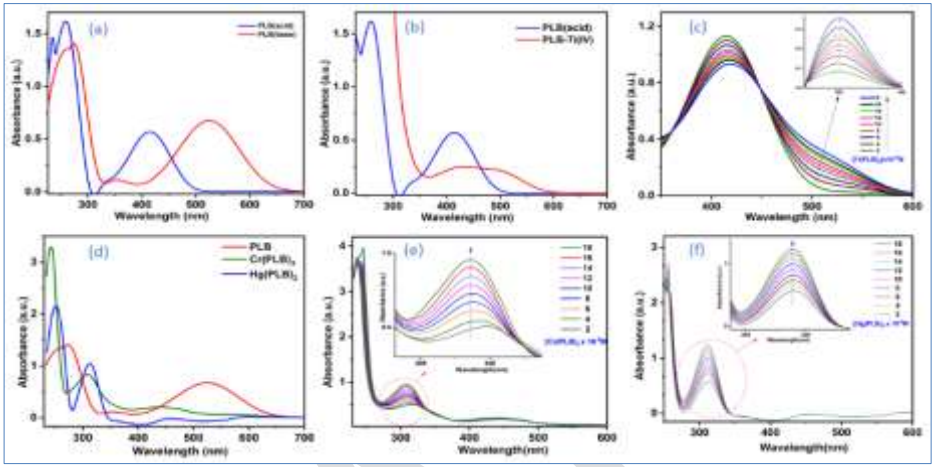


Figure 3.1. UV–Vis spectra of: (a) PLB in acidic/basic media (EtOH–H_2O); (b) PLB and $Ti(PLB)_2$ complex (pH = 5); (c) $Ti(PLB)_2$ complex at increasing concentrations (pH = 5); (d) Absorption spectra of PLB, $Cr(PLB)_3$, and $Hg(PLB)_2$ (pH = 6.5); (e) $Cr(PLB)_3$ complex at increasing concentrations; (f) $Hg(PLB)_2$ complex at increasing concentrations dần

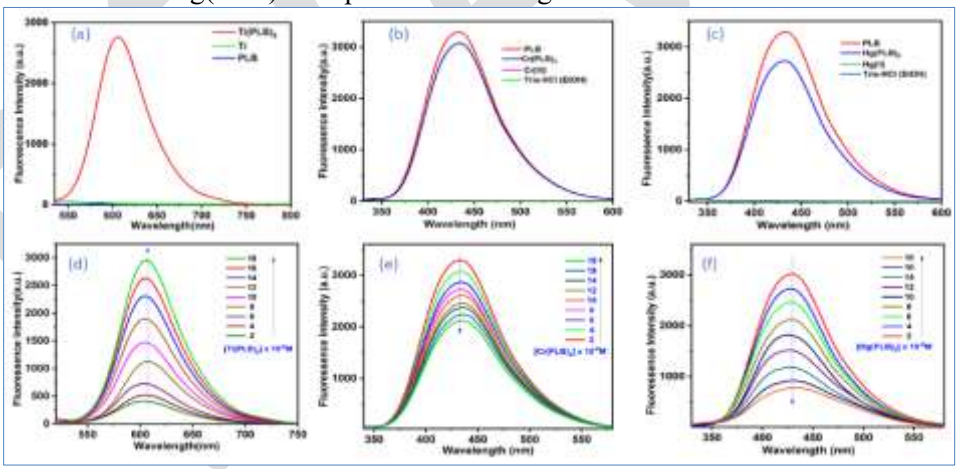


Figure 3.2. Fluorescence spectra of: (a) PLB, Ti(IV), and $Ti(PLB)_2$ (λ_{ex} = 500 nm, pH = 5); (b) PLB, Cr(III), and $Cr(PLB)_3$ (λ_{ex} = 310 nm, pH = 6.5); (c) PLB, Hg(II), and $Hg(PLB)_2$ (λ_{ex} = 310 nm, pH = 6.5); (d) $Ti(PLB)_2$ at increasing concentrations (pH = 5); (e) $Cr(PLB)_3$ at increasing concentrations (pH = 6.5); (f) $Hg(PLB)_2$ at increasing concentrations.

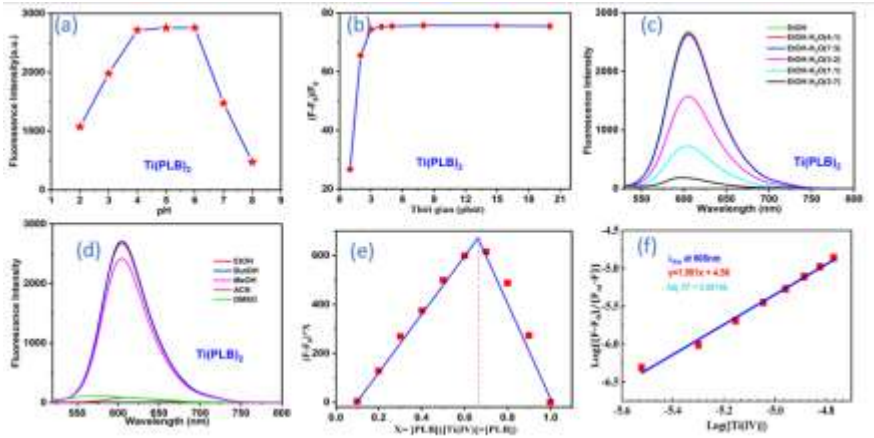


Figure 3.3. Factors affecting the formation of the $Ti(PLB)_2$ complex: (a) pH; (b) reaction time; (c) EtOH–H_2O ratio; (d) type of solvent; (e) Job's plot; (f) Benesi–Hildebrand plot (λex = 500 nm, λem = 605 nm).

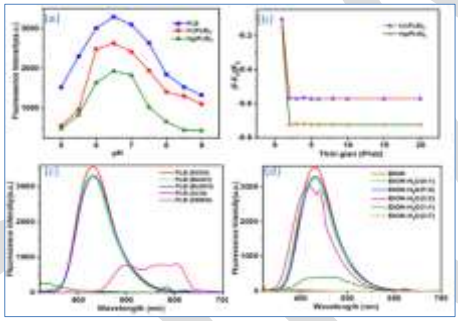


Figure 3.4. Factors affecting the formation of $Cr(PLB)_3$ and $Hg(PLB)_2$ complexes: (a) pH; (b) reaction time; (c) type of solvent; (d) EtOH:H_2O ratio (λ_{ex} = 310 nm, λ_{em} = 436 nm)

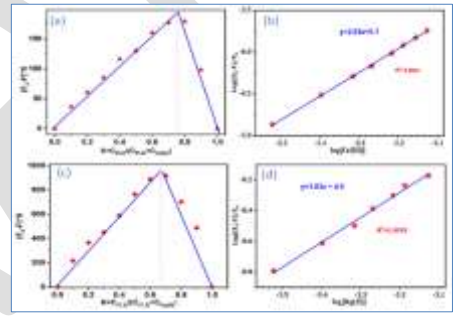


Figure 3.5. Composition and stability constants: (a, c) Job's plot of $Cr(PLB)_3$ and $Hg(PLB)_2$; (b, d) Benesi–Hildebrand plots for determining the binding constant (K) of $Cr(PLB)_3$ and $Hg(PLB)_2$

The results indicate the successful formation of three complexes: $Cr(PLB)_3$, $Hg(PLB)_2$, and $Ti(PLB)_2$. All three complexes were formed in EtOH:H_2O (7:3), yet the optimal pH values differed, reflecting variations in acid–base properties during coordination. $Ti(PLB)_2$ was most stable at pH 5, whereas $Cr(PLB)_3$ and $Hg(PLB)_2$ were stable at pH 6.5, highlighting the role of protonation state in complex formation.

$Ti(PLB)_2$ exhibited a characteristic absorption at 500 nm and emitted strong fluorescence at 605 nm. In contrast, $Cr(PLB)_3$ and $Hg(PLB)_2$ absorbed at 310 nm and quenched fluorescence with emission observed at 436 nm.

Among the three, $Cr(PLB)_3$ showed the highest binding constant (1.26×10^5), indicating strong interaction between Cr(III) and the ligand. However, due to the high-spin d^3 configuration of Cr(III), the strong spin–orbit coupling effect rapidly quenched fluorescence. Similarly, $Hg(PLB)_2$ markedly reduced fluorescence as a result of the heavy atom effect, with a relatively high binding constant (7.94×10^4). In contrast, Ti(IV), with its d^0 configuration, lacks d–d levels for non-radiative deactivation, thereby stabilizing the excited state and enabling fluorescence emission. Its relatively high binding constant (3.63×10^4) reflects stable coordination between PLB and Ti(IV), contributing to both enhanced stability and emission capability.

Overall, these results demonstrate that the fluorescence emission or quenching behavior and the stability of the complexes are not determined solely by binding strength, but are also closely linked to the electronic characteristics of the central metal ion

3.2 Characterization in the solid state, simulations, and proposed structures

The complexes $Cr(PLB)_3$, $Hg(PLB)_2$, and $Ti(PLB)_2$ were successfully synthesized through coordination reactions between PLB and the corresponding metal salts in ethanol or methanol media. The reaction conditions were optimized in terms of pH, temperature, and stirring time to obtain solid products with relatively high yields (45–56%).

After the reactions, the products were filtered, washed, dried, and characterized by modern physicochemical techniques such as FT-IR, ^{1}H-NMR, HR-MS, XRD, SEM–EDX, and theoretical simulations to elucidate their structures. The results are presented in detail in the following sections.

3.2.1 FT-IR, NMR, and HR-MS Analysis

3.2.1.1 FT-IR spectra of $Cr(PLB)_3$, $Hg(PLB)_2$, and $Ti(PLB)_2$

The FT-IR results provided clear evidence for the formation of the complexes through the shifts of the C=O stretching vibrations and the appearance of characteristic bands corresponding to metal–oxygen bonds (Ti–O, Cr–O, Hg–O). All three complexes demonstrated the coordination of PLB via both carbonyl and phenolic groups

3.2.1.2 ^{1}H-NMR, ^{13}C-NMR, HSQC, and HMBC spectra

Table 3.3. Summary of characteristic NMR signals of the three complexes

Characteristics	**Ti(PLB)$_2$**	**Cr(PLB)$_3$**	**Hg(PLB)$_2$**
Number of aromatic signals (^{1}H)	~8 signals from 6.98–7.75 ppm	~12 signals from 6.99–7.76 ppm	~8 signals from 6.99–7.75 ppm
Phenolic –OH signal (~11.97 ppm)	~11.80 ppm, indicating that PLB in the complex is not deprotonated	Absent, showing that PLB is deprotonated upon complexation	Absent, showing that PLB is deprotonated upon complexation
Aliphatic region	2.1–3.4 ppm (DMSO, CH_2; with minor impurities)	2.1–2.5 ppm (DMSO, CH_2)	2.1–2.5 ppm (DMSO, CH_2)
^{13}C-NMR	190.07 → 15.92 ppm	190.07 → 15.92 ppm	190.07 → 15.92 ppm
C=O / C–O positions	~190 ppm and ~160 ppm (present)	~190 ppm and ~160 ppm (present)	~190 ppm and ~160 ppm (present)
HSQC	Clear H–C correlations observed in both aromatic region (~7.0 ppm) and aliphatic region (~2.1–3.5 ppm)	Distinct H–C correlations in the 7.3–7.7 ppm ↔ 120–135 ppm range	Correlations observed in the aromatic region (~7 ppm) and CH_3 signal (~39 ppm)
HMBC	Long-range correlations (^{2}JCH, ^{3}JCH, sometimes ^{4}JCH)	Multiple correlations from aromatic protons to C=O and internal carbons of the ring	Long-range correlations from aromatic protons to sp² carbons and carbonyl carbons

DRAFT

3.2.2 Analysis of Elemental Composition and Oxidation States

3.2.2.1 XPS Analysis

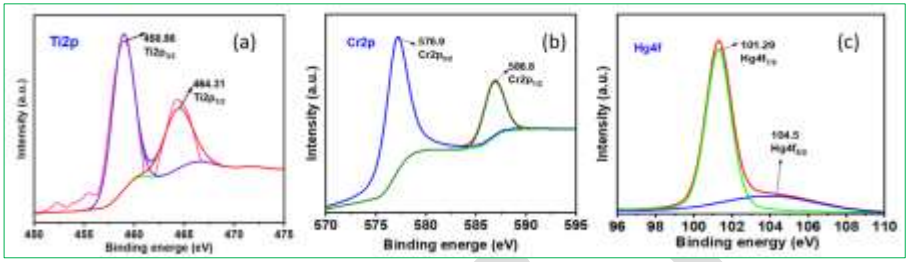


Figure 3.6. XPS spectra of the complexes: (a) $Ti(PLB)_2$; (b) $Cr(PLB)_3$; (c) $Hg(PLB)_2$.

Table 3.4. Summary of XPS analysis results of $Ti(PLB)_2$, $Cr(PLB)_3$, and $Hg(PLB)_2$ complexes

Complex	Element	Binding energy (eV)	Elemental composition (%)	Oxidation state of central ion
$Ti(PLB)_2$	C1s	283,98	75,81	Ti(IV)
	Ti2p	459,00	0,61	
	O1s	531,23	23,58	
$Cr(PLB)_3$	Cr2p	576,93	1,34	Cr(III)
	C1s	284,56	74,21	
	O1s	532,13	24,44	
$Hg(PLB)_2$	Hg4f	101,75	0,20	Hg(II)
	C1s	284,59	76,70	
	O1s	531,90	23,09	

3.2.2.2 Thermal characterization of the complexes by TGA

DRAFT

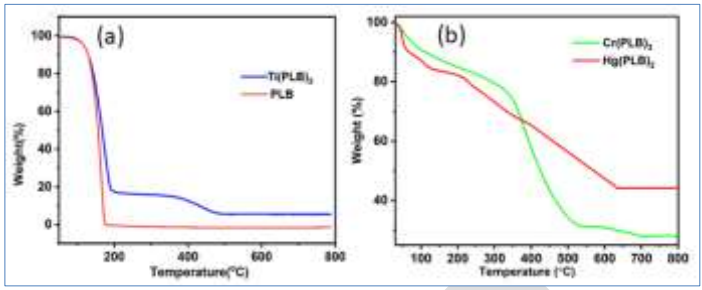


Figure 3.7. TGA curves of PLB, $Ti(PLB)_2$, $Cr(PLB)_3$, and $Hg(PLB)_2$

Thermogravimetric analysis (TGA) revealed that free PLB undergoes significant decomposition in the range of 80–200 °C, reflecting the low thermal stability typical of organic compounds. In contrast, the PLB–metal complexes exhibited higher stability:

$Ti(PLB)_2$: three distinct stages were observed, including loss of crystallization water (~110 °C), decomposition of the organic moiety (200–450°C), and formation of a stable residue identified as TiO_2.

$Hg(PLB)_2$: continuous decomposition occurred over 100–600°C without clearly separated stages, leaving a final residue (~40–45%) attributed to HgO.

$Cr(PLB)_3$: three distinct stages were evident, including water loss (50–100°C), partial decomposition of functional groups (100–300 °C), and breakdown of the naphthoquinone framework (300–480 °C), leaving Cr_2O_3 (~27–28%) as the final residue.

3.2.4 Morphology and Crystal Structure (XRD)

DRAFT

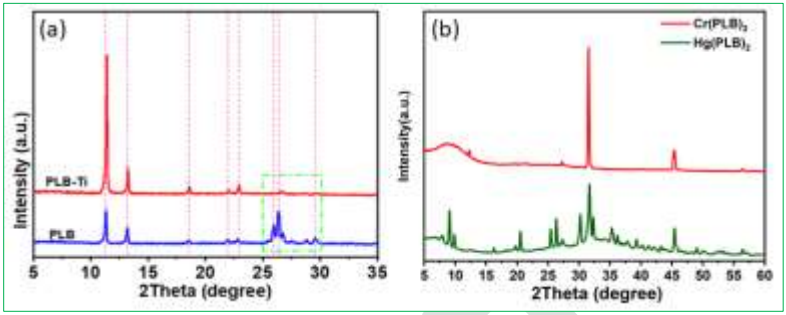


Figure 3.8. XRD patterns of free PLB and its complexes $Ti(PLB)_2$, $Cr(PLB)_3$, and $Hg(PLB)_2$

The XRD patterns revealed significant changes in the crystal structures of the PLB–metal complexes compared to free PLB. Free PLB exhibited semi-crystalline characteristics with sharp peaks in the 2θ range of 11–27°. Upon complexation:

$Ti(PLB)_2$: new peaks appeared while several original peaks disappeared, indicating a reduction in crystallinity and a tendency toward an amorphous structure.

$Cr(PLB)_3$: multiple intense peaks were observed (2θ = 9.87°, 27.3°, 31.4°, 33.6°, 45.6°…), confirming the formation of a new crystalline phase with a stable octahedral coordination model.

$Hg(PLB)_2$: displayed an intermediate nature, with both crystalline peaks (2θ = 9.12°, 26.86°, 31.6°…) and amorphous regions.

These results demonstrate that metal ion coordination markedly alters the crystal lattice: $Cr(PLB)_3$ exhibited the highest crystallinity, $Ti(PLB)_2$ was largely amorphous, while $Hg(PLB)_2$ showed a moderate degree of crystallinity.

3.2.5 Optimized Geometrical Structures by DFT

DRAFT

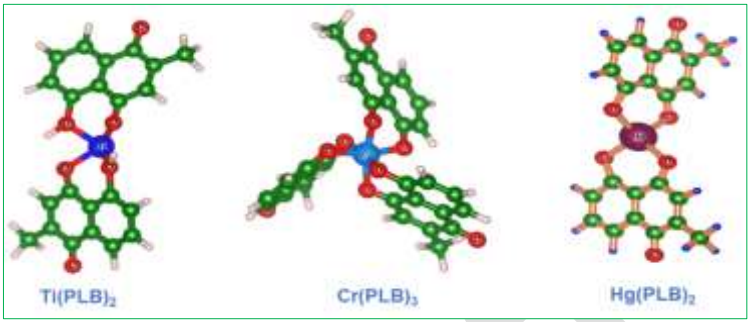


Figure 3.9. Optimized structures of $Ti(PLB)_2$, $Cr(PLB)_3$, and $Hg(PLB)_2$ complexes

DFT optimization (B3LYP/6-31G(d,p), LANL2DZ, PCM model) revealed significant geometric differences depending on the central metal ion. The metal ions coordinated with the –OH and C=O groups of PLB, forming:

$Ti(PLB)_2$: distorted tetrahedral geometry (d^0 configuration);

$Cr(PLB)_3$: distorted octahedral geometry (d^3 configuration);

$Hg(PLB)_2$: distorted tetrahedral geometry (d^{10} configuration), influenced by the presence of a lone electron pair.

The M–O bond lengths decreased in the order Hg(II) > Ti(IV) > Cr(III) (1.83–2.19 Å), consistent with ionic radii and electron-sharing tendencies. Mulliken charge analysis indicated that Cr(III) had the strongest electron-accepting ability, resulting in shorter and more stable bonds.

The DFT results were in good agreement with FT-IR, XPS, and SEM–EDX analyses, confirming the proposed structural models and highlighting the interaction trend: Cr(III) > Ti(IV) > Hg(II).

DRAFT

3.2.6 Electronic parameters obtained from DFT calculations

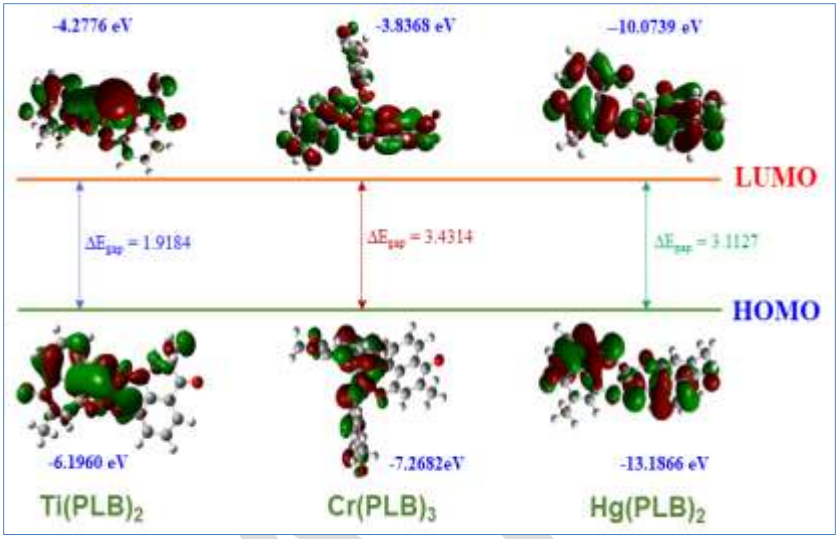


Figure 3.10. HOMO–LUMO representation and ΔEgap values of $Ti(PLB)_2$, $Cr(PLB)_3$, and $Hg(PLB)_2$ complexes

The HOMO–LUMO energy gaps (ΔEgap) were determined as follows: $Cr(PLB)_3$ (3.43 eV) > $Hg(PLB)_2$ (3.11 eV) > $Ti(PLB)_2$ (1.92 eV). Mulliken/NBO analyses revealed that $Cr(PLB)_3$ possessed the highest number of donor→acceptor interactions but with relatively low stabilization energy E(2) (14.2 kcal/mol), and a higher positive charge on Cr (+1.41), indicating weaker bonding. $Ti(PLB)_2$ exhibited the highest stabilization energy E(2) (18.5 kcal/mol) and a charge of +1.26, suggesting more effective coordination. $Hg(PLB)_2$ showed E(2) = 16.8 kcal/mol and a charge of +1.18, but was influenced by relativistic effects characteristic of Hg.

The stability order was therefore established as Ti(IV) > Hg(II) > Cr(III), consistent with FT-IR, XPS, DFT, and fluorescence data.

The $Ti(PLB)_2$, $Cr(PLB)_3$, and $Hg(PLB)_2$ complexes were successfully synthesized in the solid state, with stable structures, providing a solid foundation for further studies on fluorescence sensing and subsequent applications

3.3 Mechanistic study and proposed structures of the complexes.

3.3.1 Complex formation and proposed structures

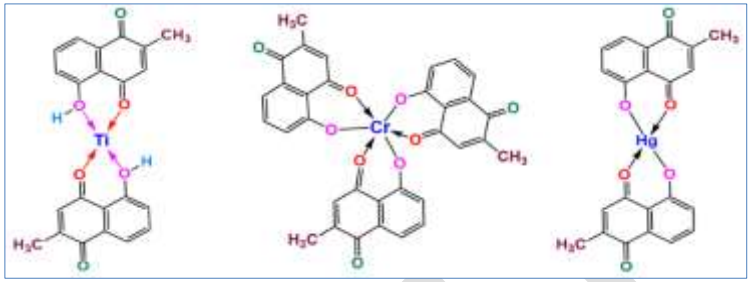


Figure 3.11. Proposed structures of $Ti(PLB)_2$, $Cr(PLB)_3$, and $Hg(PLB)_2$ complexes

Coordination mechanism: PLB forms M–O bonds through donor–acceptor interactions LP(O) → d*(M), in which the donor is the lone pair of the hydroxyl and carbonyl groups, and the acceptor is the vacant d orbital of the metal ion.

NBO/DFT analysis:

Ti(IV) (d^0): strongest interaction, E(2) ≈ 18.5 kcal/mol → stable coordination, enhanced emission capability.

Cr(III) (d^3): lower E(2) (~14.2 kcal/mol) → weaker coordination, prone to triplet-state transitions.

Hg(II) (d^{10}): intermediate E(2) (~16.8 kcal/mol), affected by the heavy atom effect → fluorescence quenching tendency.

Mulliken analysis: high positive charges on the metals (+1.18 to +1.41) indicate strong electron-withdrawing behavior and bond polarization.

The bonding nature in these complexes is dominated by donor–acceptor interactions of the LP(O) → d*(M) type, which govern their geometries, stability, and photophysical–biological properties.

DRAFT

3.3.2 Discussion on the emission and quenching mechanisms of the complexes

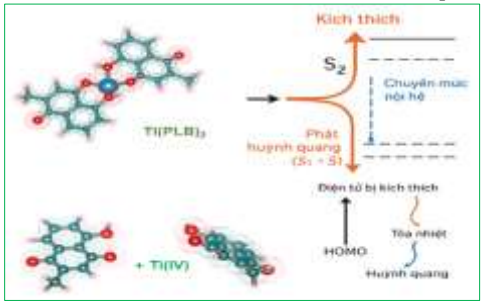


Figure 3.12. Fluorescence emission mechanism of Ti(PLB)$_2$

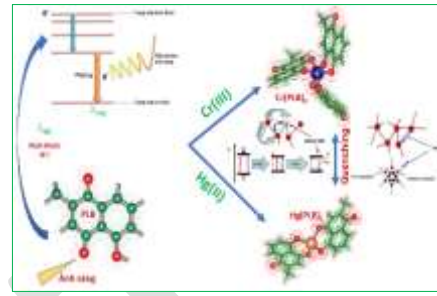


Figure 3.13. Emission and quenching mechanisms of PLB upon complexation with Cr(III) and Hg(II)

Ti(PLB)$_2$ exhibits strong fluorescence. Absorption occurs mainly through the π–π* transition of PLB ($\lambda_{ex} \approx 500$ nm), followed by emission at 600–646 nm with a large Stokes shift. A CHEF (Chelation-Enhanced Fluorescence) effect is observed: complexation with Ti(IV) rigidifies the structure, reduces intramolecular vibrations, and enhances emission efficiency [9][10]. Ti(IV) (d^0, non-magnetic) stabilizes the excited state against solvent-induced quenching [11]. The $\Delta E_{gap} \approx 1.92–2.15$ eV and favorable orbital distribution allow asymmetric electronic transitions, thereby intensifying fluorescence.

Cr(PLB)$_3$ and Hg(PLB)$_2$ induce fluorescence quenching. Their large ΔE_{gap} values (3.43 eV and 3.11 eV, respectively) hinder electron transfer and emission. Cr(III), with a high Mulliken charge (+1.41), induces strong bond polarization and geometric distortion, leading to enhanced non-radiative dissipation of energy [12]. Hg(II), being a heavy atom with a d^{10} configuration, promotes strong spin–orbit coupling, facilitating intersystem crossing (ISC) and thereby quenching fluorescence. Stern–Volmer experiments showed very high Ksv and Kq values, confirming a static quenching mechanism through the formation of non-emissive complexes.

DRAFT

3.4 Analytical applications and evaluation of biological activities

3.4.1 Evaluation of the biological activities of $Cr(PLB)_3$ and $Hg(PLB)_2$ complexes

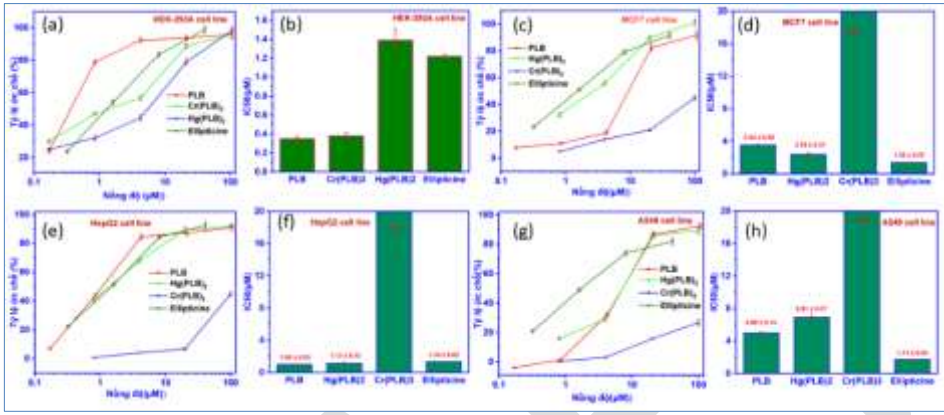


Figure 3.14. Cytotoxic effects of PLB, $Cr(PLB)_3$, $Hg(PLB)_2$, and ellipticine on human embryonic kidney HEK-293A cells (a–b) and three human cancer cell lines: MCF-7 (c–d), HepG2 (e–f), and A549 (g–h). (a, c, e, g): % inhibition versus concentration. (b, d, f, h): Corresponding IC_{50} values (μM).

The $Hg(PLB)_2$ complex exhibited remarkable efficacy against the MCF-7 cell line while showing lower toxicity toward normal cells compared to free PLB. In contrast, although $Cr(PLB)_3$ displayed high toxicity toward HEK-293A, it showed almost no inhibitory effect on the examined cancer cell lines. These findings suggest that the nature of the central ion may exert opposite influences on biological activity, depending on the specific molecular interaction mechanisms.

3.4.2 Interaction with HSA and enzyme docking of $Cr(PLB)_3$ and $Hg(PLB)_2$ complexes

Comprehensive results from UV–Vis, FT–IR, fluorescence, ^{1}H-NMR, CD, FRET, and thermodynamic analyses indicated that both $Cr(PLB)_3$ and $Hg(PLB)_2$ formed stable complexes with HSA through noncovalent interactions such as hydrogen bonding, van der Waals forces, and hydrophobic interactions. Both complexes were found to bind at Sudlow site I, the major drug-binding site in plasma.

Notably, $Hg(PLB)_2$ not only exhibited strong biological activity against cancer cell lines and the α-glucosidase enzyme, but also demonstrated effective

interaction with HSA, with stable binding parameters, appropriate FRET distances, and moderate structural alterations. These factors suggest that $Hg(PLB)_2$ holds promising potential as a therapeutic agent or biocarrier system, capable of efficient transport in plasma.

By contrast, although $Cr(PLB)_3$ did not display significant biological efficacy, it induced pronounced alterations in the secondary structure of HSA, particularly reducing α-helix content and shifting the intrinsic fluorophore. This reflects the strong coordination tendency of Cr(III) ions with proteins, shedding light on the binding mechanism of d^3 metal ions with serum albumins..

3.4.3 Application of the $Ti(PLB)_2$ complex in the fluorescence determination of Ti(IV)

3.4.3.1 Effect of interfering ions

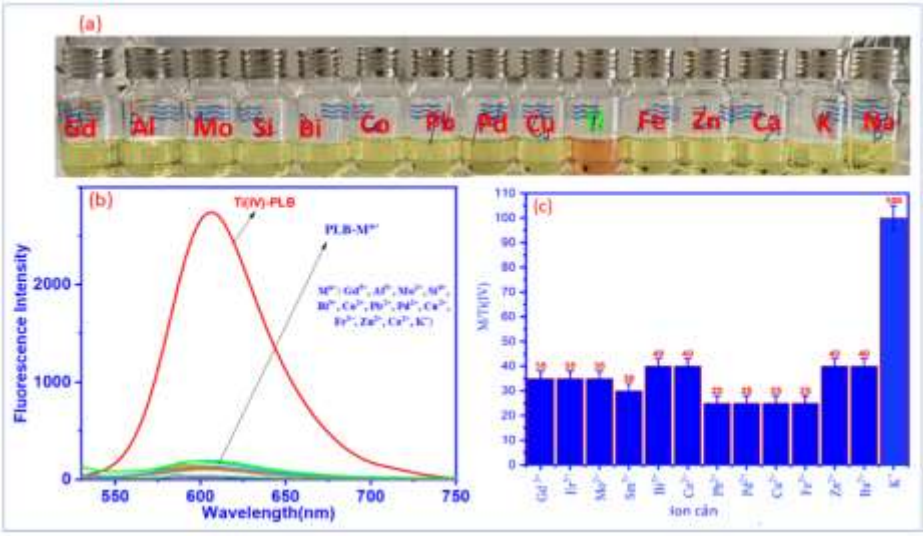


Figure 3.43. Fluorescence selectivity of PLB toward Ti(IV): (a) Photographs of PLB samples after addition of various metal ions; (b) Fluorescence spectra of the Ti(IV)–PLB complex compared with PLB–M^{n+}; (c) Comparison chart of [M]/[Ti(IV)] ratios affecting the fluorescence intensity of the $Ti(PLB)_2$ complex.

Only the $Ti(PLB)_2$ complex exhibited strong fluorescence at 605 nm; other metal ions (Na^+, K^+, Ca^{2+}, Zn^{2+}, Fe^{3+}, Cu^{2+}, Pb^{2+}, Co^{2+}, Pd^{2+}, Bi^{3+}, Si^{4+}, Mo^{2+}, Al^{3+}, Gd^{3+}) produced negligible fluorescence signals → confirming high selectivity toward Ti(IV). Alkali, alkaline earth, and rare-earth ions (Na^+, K^+, Ca^{2+}, Gd^{3+}, etc.) showed almost no interference, even at concentrations 100 times higher than Ti(IV). Some transition metal ions (Fe^{3+}, Cu^{2+}, Zn^{2+}, Pb^{2+}) caused significant quenching only at [M]/[Ti] ratios of 25–40.

In real sand samples, the major coexisting ions (Si, Al, Fe, Ca, K, Na, Mg) showed low interference levels; in particular, Fe^{3+} reduced the fluorescence intensity by only ~25%.

Conclusion: The $Ti(PLB)_2$ complex demonstrated high selectivity and strong anti-interference ability, making it suitable for Ti(IV) analysis in complex matrices such as sand.

3.4.3.2 Determination of LOD and LOQ

The method gave an LOD = 2.0×10^{-7} M and an LOQ = 6.69×10^{-7} M, with R^2 = 0.9962. The RSD was 4.09%, and the recovery rate reached 103%. These results indicate that the method possesses high sensitivity and accuracy, making it suitable for the quantification of Ti(IV) under optimized conditions.

3.4.3.2 Application to real sand sample analysis

Table 3.13. Determination of Ti content in Binh Thuan sand samples

Sample	Proposed method (µM)	ICP–OES method* (µM)	Relative error (%)
BT1	3.13 ± 0.02	3.05 ± 0.04	2.62%
BT2	3.00 ± 0.07	3.11 ± 0.06	–3.54 %
BT3	3.25 ± 0.04	3.17 ± 0.02	2.52%
BT4	3.32 ± 0.06	3.35 ± 0.06	–0.90 %
BT5	3.08 ± 0.03	3.12 ± 0.06	–1.28 %

3.4.4 Application of the $Hg(PLB)_2$ complex in the quantification of Hg(II) by HPLC–DAD

This study successfully developed an HPLC–DAD analytical method based on the $Hg(PLB)_2$ complex, enabling rapid and efficient determination of Hg(II) in environmental samples. The optimized chromatographic conditions and performance parameters of the method are summarized in Table 3.22.

Table 3.22. Summary of optimized conditions and characteristics of the HPLC–DAD method using the $Hg(PLB)_2$ complex for Hg(II) analysis

Criterion	Content
Method name	HPLC–DAD using the $Hg(PLB)_2$ complex
Application	Determination of Hg(II) in environmental samples
Optimized chromatographic conditions	- Detection wavelength: 224 nm - pH: 6.0 - Mobile phase: H_2O:EtOH = 1:1 (v/v) - Column temperature: 40 °C
Method characteristics	- LOD: 5.0 µg/L - LOQ: 20.0 µg/L - High linearity: $R^2 > 0.994$ - Good repeatability, meeting AOAC standards
Comparison with ICP–MS	Low deviation, consistent results
Outstanding advantages	- Environmentally friendly - Short analysis time (~2–3 min) - Low cost, suitable for budget-limited laboratories or field applications
Practical applications	- Surface water analysis - Button batteries; Fluorescent lamps
General conclusion	An effective and reliable alternative method to ICP–MS for Hg(II) analysis

DRAFT

CONCLUSIONS AND RECOMMENDATIONS

1. Conclusions

This dissertation investigated the complexation of PLB with Cr(III), Hg(II), and Ti(IV). The main findings can be summarized as follows:

For the first time, three complexes $Cr(PLB)_3$, $Hg(PLB)_2$, and $Ti(PLB)_2$ were successfully synthesized. The coordination stoichiometries were determined as 1:3 (for the Cr complex) and 1:2 (for the Hg(II) and Ti(IV) complexes) with PLB, confirmed through common laboratory spectroscopic methods.

The interaction mechanisms of PLB with the metal ions were elucidated. $Ti(PLB)_2$ exhibited strong fluorescence emission due to structural rigidification and reduced non-radiative vibrations, while $Cr(PLB)_3$ and $Hg(PLB)_2$ caused static quenching, as confirmed by Stern–Volmer plots, UV–Vis spectra, and DFT simulations. Solid-state analyses and DFT modeling demonstrated coordination via the –OH and =O groups of PLB, forming distorted octahedral geometry (Cr(III)) or distorted tetrahedral geometry (Ti(IV), Hg(II)).

The biological applications were confirmed by in vitro studies, highlighting anticancer and antidiabetic potential. These findings were consistent with molecular docking and MD simulations, which revealed stable binding at the Trp214 site of HSA and at target enzymes (Topoisomerase, Bcl-2, α-glucosidase).

$Ti(PLB)_2$ induced strong fluorescence, opening avenues for quantitative analysis. A quantification protocol was established based on complex formation: $Ti(PLB)_2$ enabled highly sensitive determination of Ti(IV) (LOD ~10^{-7} M), successfully applied to sand samples.

$Cr(PLB)_3$ and $Hg(PLB)_2$ exhibited fluorescence quenching, confirming stable complex formation and providing potential applications in biological studies and fluorescence probes. $Hg(PLB)_2$ was successfully applied to the quantification of Hg(II) by HPLC–DAD, with stable retention time, LOD 0.25 µM, good reproducibility (RSD < 2%), and high selectivity. Additionally, fluorescence quenching supported studies of interactions with HSA, indicating the potential to explore Cr(III) and Hg(II) complexes for drug transport research.

New contributions of the dissertation

For the first time, three complexes $Ti(PLB)_2$, $Cr(PLB)_3$, and $Hg(PLB)_2$ were successfully synthesized and characterized in both solution and solid state by integrating experimental methods (UV–Vis, fluorescence, FT-IR, XRD, XPS, etc.) with theoretical modeling (DFT, docking, MD).

The biological potential of the complexes was identified, particularly their anticancer and antidiabetic activities, with implications for drug delivery studies and interactions with carrier proteins.

The fluorescence and HPLC–DAD methods were successfully applied for selective and accurate quantification of Ti(IV) and Hg(II) ions via their respective complexes, paving the way for the development of chemical probes and trace metal analysis.

2. Recommendations

Within the scope of this dissertation, only certain properties and applications of the complexes were investigated. Further studies should expand in the following directions:

Conduct deeper investigations into biological mechanisms, including in vitro tests (interactions with real cells and enzymes) to evaluate anti-inflammatory and anticancer effects of the complexes.

Extend simulations of interactions with specific biological targets (e.g., DNA, human albumin, cancer cell receptors) to clarify molecular-level mechanisms.

Explore the use of PLB as a sensitive probe for detecting Cr(III) and Hg(II).

Design new PLB derivatives by structural modifications (e.g., methylation, halogenation) to study the effects of substituents on complexation ability, selectivity, and emission properties, thereby developing improved reagents with optimized sensitivity and biological applications.

Develop solid-state sensors (thin films or test papers) incorporating $Ti(PLB)_2$ or Cr/Hg-based probes for rapid field detection using portable fluorescence devices, with potential applications in environmental monitoring and biomedical analysis..

.

DRAFT

TÀI LIỆU THAM KHẢO

[1] S. Salunke-Gawali, E. Pereira, U. A. Dar, and S. Bhand, "Metal complexes of hydroxynaphthoquinones: Lawsone, bis-lawsone, lapachol, plumbagin and juglone," Nov. 15, 2017, *Elsevier B.V.* doi: 10.1016/j.molstruc.2017.06.130.

[2] K. Satheeshkumar, B. Jose, B. P. Dhanya, and P. N. Krishnan, "Prospects of Plumbago rosea L. hairy root culture in traditional preparations: A phytochemical comparison with tuberous roots," *Plant Root*, vol. 8, pp. 13–23, Sep. 2014, doi: 10.3117/plantroot.8.13.

[3] Havel and Peter J, "A scientific review: the role of chromium in insulin resistance," *The Science of Diabetes Self-Management and Care, Suppl(3 SUPPL.)*, no. 2635–0106, 2004.

[4] T. W. Clarkson, L. Magos, and G. J. Myers, "The Toxicology of Mercury-Current Exposures and Clinical Manifestations," 2003. [Online]. Available: www.nejm.org

[5] M. D. Vasudevarao *et al.*, "Naphthoquinone-mediated inhibition of lysine acetyltransferase KAT3B/p300, basis for non-toxic inhibitor synthesis," *Journal of Biological Chemistry*, vol. 289, no. 11, pp. 7702–7717, Mar. 2014, doi: 10.1074/jbc.M113.486522.

[6] D. Sajan, K. P. Laladhas, I. Hubert Joe, and V. S. Jayakumar, "Vibrational spectra and density functional theoretical calculations on the antitumor drug, plumbagin," *Journal of Raman Spectroscopy*, vol. 36, no. 10, pp. 1001–1011, 2005, doi: 10.1002/jrs.1398.

[7] Z.-F. Chen *et al.*, "Cytotoxicity of the traditional chinese medicine (TCM) plumbagin in its copper chemistry," *Dalton Transactions*, no. 48, p. 10824, 2009, doi: 10.1039/b910133k.

[8] S. Mukherjee, A. V. Sawant, S. S. Prassanawar, and D. Panda, "Copper-Plumbagin Complex Produces Potent Anticancer Effects by Depolymerizing Microtubules and Inducing Reactive Oxygen Species and DNA Damage," *ACS Omega*, 2022, doi: 10.1021/acsomega.2c06691.

[9] D. Wu, A. C. Sedgwick, T. Gunnlaugsson, E. U. Akkaya, J. Yoon, and T. D. James, "Fluorescent chemosensors: the past, present and future," *Chem*

Soc Rev, vol. 46, no. 23, pp. 7105–7123, 2017, doi: 10.1039/C7CS00240H.

[10] H. N. Kim, M. H. Lee, H. J. Kim, J. S. Kim, and J. Yoon, "A new trend in rhodamine-based chemosensors: application of spirolactam ring-opening to sensing ions," *Chem Soc Rev*, vol. 37, no. 8, p. 1465, 2008, doi: 10.1039/b802497a.

[11] Q. Zhao, C. Huang, and F. Li, "Phosphorescent heavy-metal complexes for bioimaging," *Chem Soc Rev*, vol. 40, no. 5, p. 2508, 2011, doi: 10.1039/c0cs00114g.

[12] G. Colombo, G. Attilio Ardizzoia, J. Furrer, B. Therrien, and S. Brenna, "Driving the Emission Towards Blue by Controlling the HOMO-LUMO Energy Gap in BF_2 -Functionalized 2-(Imidazo[1,5-*a*]pyridin-3-yl)phenols," *Chemistry – A European Journal*, vol. 27, no. 48, pp. 12380–12387, Aug. 2021, doi: 10.1002/chem.202101520.

DRAFT